



# Multiscale imaging of basal cell dynamics in the functionally mature mammary gland

Alexander J. Stevenson<sup>a,b,1</sup>, Gilles Vanwalleghem<sup>c,1</sup>, Teneale A. Stewart<sup>a,b</sup>, Nicholas D. Condon<sup>d</sup>, Bethan Lloyd-Lewis<sup>e</sup>, Natascia Marino<sup>f,g</sup>, James W. Putney<sup>h</sup>, Ethan K. Scott<sup>c</sup>, Adam D. Ewing<sup>a,b</sup>, and Felicity M. Davis<sup>a,b,2</sup>

<sup>a</sup>Faculty of Medicine, Mater Research Institute, The University of Queensland, Brisbane, QLD 4102, Australia; <sup>b</sup>Translational Research Institute, Woolloongabba, QLD 4102, Australia; <sup>c</sup>Queensland Brain Institute, The University of Queensland, Brisbane, QLD 4072, Australia; <sup>d</sup>Institute for Molecular Bioscience, The University of Queensland, Brisbane, QLD 4072, Australia; <sup>e</sup>School of Cellular and Molecular Medicine, University of Bristol, Bristol BS8 1TD, United Kingdom; <sup>f</sup>Susan G. Komen Tissue Bank at IU Simon Cancer Center, Indiana University School of Medicine, Indianapolis, IN 46202; <sup>g</sup>Department of Medicine, Indiana University School of Medicine, Indianapolis, IN 46202; and <sup>h</sup>National Institute of Environmental Health Sciences, National Institutes of Health, Research Triangle Park, NC 27709

Edited by Bertil Hille, University of Washington School of Medicine, Seattle, WA, and approved September 10, 2020 (received for review August 17, 2020)

**The mammary epithelium is indispensable for the continued survival of more than 5,000 mammalian species. For some, the volume of milk ejected in a single day exceeds their entire blood volume. Here, we unveil the spatiotemporal properties of physiological signals that orchestrate the ejection of milk from alveolar units and its passage along the mammary ductal network. Using quantitative, multidimensional imaging of mammary cell ensembles from GCaMP6 transgenic mice, we reveal how stimulus evoked Ca<sup>2+</sup> oscillations couple to contractions in basal epithelial cells. Moreover, we show that Ca<sup>2+</sup>-dependent contractions generate the requisite force to physically deform the innermost layer of luminal cells, compelling them to discharge the fluid that they produced and housed. Through the collective action of thousands of these biological positive-displacement pumps, each linked to a contractile ductal network, milk begins its passage toward the dependent neonate, seconds after the command.**

calcium signaling | GCaMP6 | mammary gland | lactation | oxytocin

The mammary gland has a central role in the health and survival of all mammals (1, 2). Development of this organ is a multistep process that begins as the female embryo develops in her mother's uterus (2, 3) and culminates as she nurtures the next generation of offspring in her own (2, 4). In mice, the postpubertal female mammary gland consists of an elaborate network of evenly spaced branching ducts embedded within an adipocyte-rich stroma (4). Each mammary duct consists of an inner layer of heterogeneous luminal epithelial cells, which include both estrogen receptor (ER)-positive and -negative cell lineages (5, 6). These cells are surrounded by a layer of basal epithelial cells, which express the basal cytokeratins K5 and K14 as well as smooth muscle actin (SMA) (7, 8). Heterogeneity also exists within the basal cell compartment, with recent single-cell RNA sequencing confirming clusters of cells with high levels of the genes encoding SMA, oxytocin receptor (OXTR), and K15 (termed basal myoepithelial cells) as well as a population of cells with high levels of *Procr*, *Gng11*, and *Zeb2* (termed basal Procr<sup>+</sup> cells) (7).

During alveologenesis in pregnancy, adult mammary stem and progenitor cells rapidly proliferate to generate the millions of new cells that are required to produce, store, and expel milk during lactation (9, 10). These cells are arranged in mammary alveoli, with each alveolar unit broadly consisting of an inner layer of secretory luminal cells and an outer network of contractile basal cells (4). Many alveolar units cluster to form large lobuloalveolar complexes, which connect to each other and to the nipple via the tubular ductal network. The development and function of epithelial cells in the mammary gland during pregnancy and lactation are governed by a range of local and systemic factors (11). A greater appreciation of these factors, and the molecular pathways that link signal reception to cellular outcomes,

would greatly improve our understanding of this fundamental process in mammalian biology.

The ability to visualize how a single living cell, in its native environment, translates an extracellular message into an intracellular signal to execute a defined task at the cell level and cooperatively achieve a biological outcome at the organ level is revolutionizing our understanding of multicellular systems. Such an approach has provided new insights into a range of biological phenomena, including how plants defend against herbivory (12), how fish escape looming predators (13, 14), and how mammals store memories (15). The rational design and continued refinement of genetically encoded Ca<sup>2+</sup> indicators (GECIs) has fueled these advances (16). However, the use of GECIs for in situ activity mapping in adult vertebrates, has largely remained an achievement of neuroscience, where neural activity is tightly coupled to intracellular Ca<sup>2+</sup> ([Ca<sup>2+</sup>]<sub>i</sub>) signaling (17).

Efforts to map activity networks in specific populations of nonexcitable cells in other solid organs is lagging. Indeed, our understanding of signal transduction in many epithelial tissue types (including the mammary gland) has principally arisen through analysis of isolated cells (often serially propagated under physiologically extraneous conditions), retrospective examination

## Significance

**The mammary gland is functional for only a brief period of a female's lifetime. During this time, it operates not for the survival of the individual, but for the survival of her species. Here, we visualize the nature of alveolar contractions in the functionally mature mammary gland, revealing how specialized epithelial cells, which possess the ability to behave like smooth muscle cells, undergo Ca<sup>2+</sup>-dependent contractions. We demonstrate that individual oscillators can be electrically coupled to achieve global synchrony, a phenomenon that has not yet been observed in the mammary gland. By imaging activity across scales, we provide a window into the organization, dynamics, and role of epithelial Ca<sup>2+</sup> oscillations in the organ principally responsible for sustaining neonatal life in mammals.**

Author contributions: A.J.S., G.V., T.A.S., B.L.-L., J.W.P., and F.M.D. designed research; A.J.S., T.A.S., and F.M.D. performed research; N.M. contributed new reagents/analytic tools; A.J.S., G.V., T.A.S., N.D.C., E.K.S., A.D.E., and F.M.D. analyzed data; and F.M.D. wrote the paper.

The authors declare no competing interest.

This article is a PNAS Direct Submission.

Published under the PNAS license.

<sup>1</sup>A.J.S. and G.V. contributed equally to this work.

<sup>2</sup>To whom correspondence may be addressed. Email: f.davis@uq.edu.au.

This article contains supporting information online at <https://www.pnas.org/lookup/suppl/doi:10.1073/pnas.2016905117/-DCSupplemental>.

First published October 8, 2020.

of fixed tissue, and interrogation of genetic knockout models (where biological function is inferred in the absence of physiological redundancy or compensation). The ability to visualize signal–response relationships in mammary epithelial cells in situ and across scales will shed important new light on both structure–function relationships and patterns of cellular connectivity in this important epithelial organ.

When young offspring suckle, maternally produced oxytocin (OT) binds to its cognate receptor (the OXTR) on mammary basal cells, causing them to contract (18). Activity is likely to be tightly coupled to  $[Ca^{2+}]_i$  in these cells via a phospholipase C (PLC)-inositol trisphosphate (InsP3) signaling pathway (18–22). The absence of physiological redundancy in the mammary OT/OXTR system—highlighted by the inability of both OT ligand- and receptor-null mice to adequately nurse their pups (23–25) [a phenotype that can be rescued in ligand-null animals through administration of exogenous OT (24)]—facilitates the direct visualization of this specific epithelial signal–response relationship at this important stage of development.

In this study, we engineered mice with directed expression of a GECI to basal epithelial cells in the mammary gland. This enabled us to quantitatively probe the organization and function of real-time  $[Ca^{2+}]_i$  signaling events in individual cells within this complex living tissue, at a level of rigor that has only previously been achieved in the adult brain.

## Results

**Basal Cell  $[Ca^{2+}]_i$  Oscillations Signal to Repetitively Deform Mammary Alveoli and Force Milk Out.** We developed transgenic mice that express the fast, ultrasensitive GECI GCaMP6f (16) under the inducible control of the K5 gene promoter (8) (*GCaMP6f;K5CreERT2* mice) (Fig. 1A). The relatively high baseline fluorescence of this GECI is well suited for the quantitative assessment of  $[Ca^{2+}]_i$  responses in alveolar basal cells, which are sparsely distributed with thin cellular processes (16, 26) (*SI Appendix, Fig. S1A and B*). GCaMP6f consists of a circularly permuted green fluorescent protein (GFP), enabling three-dimensional (3D) assessment of its expression and lineage-specific localization using an anti-GFP antibody (27) and optimized methods for tissue clearing (28). Genetic recombination in this model was high (*SI Appendix, Fig. S2A and B*) and showed lineage restriction to basal epithelial cells (Fig. 1B).

To assess OT-mediated basal cell  $[Ca^{2+}]_i$  responses, we performed four-dimensional (4D) ( $x$ ,  $y$ ,  $z$ , and  $t$ ) imaging of ex vivo mammary tissue pieces from lactating *GCaMP6f;K5CreERT2* mice—a method similar to the preparation of acute brain slices for neural imaging (*SI Appendix, Methods*) (29). Tissue was loaded with the live cell permeable dye CellTracker Red to visualize alveolar luminal (milk producing) cells (*SI Appendix, Fig. S1A*). A coordinated wave of  $[Ca^{2+}]_i$ , due to InsP3-mediated endoplasmic reticulum (ER)  $Ca^{2+}$  store release (18, 19, 22), was observed in mammary basal cells following OT stimulation and its diffusion through the tissue (Fig. 1C and *Movie S1*). This initial transient  $[Ca^{2+}]_i$  elevation was followed by a phase of stochastic  $[Ca^{2+}]_i$  oscillations (Fig. 1C arrowheads and *Movie S1*) that were likely to be sustained in part by  $Ca^{2+}$  influx across the plasma membrane (19, 21, 30).

The organization of basal cell contractions was also examined using 3D, deep tissue imaging of myosin light chain (MLC) phosphorylation. In tissue treated with OT prior to fixation, phospho-MLC (pMLC)-positive and -negative basal cells were observed to be interspersed throughout alveolar clusters (Fig. 1D), supporting the ostensibly stochastic nature of the mammary contractile response. Regions containing clusters of pMLC-positive cells, however, were also observed in OT-treated tissue (see *SI Appendix, Fig. S3A* asterisk and *SI Appendix, Fig. S3B*). Intravital imaging of OT-mediated  $[Ca^{2+}]_i$  responses (31)

supported observations in acute ex vivo tissue preparations (*SI Appendix, Fig. S4A–C* and *Movie S2*).

To determine whether increases in  $[Ca^{2+}]_i$  are temporally correlated with alveolar unit contractions, we quantified  $Ca^{2+}$ -contraction responses in alveolar tissue. While cell- and tissue-level movement is physiologically relevant and important, it poses additional computational challenges to the analysis of single-cell  $Ca^{2+}$  responses in 4D image sequences. To overcome this, we utilized the diffeomorphic registration approach of Advanced Normalization Tools for motion correction (32, 33) (*SI Appendix, Methods*). This approach corrected major tissue movements; however, alveolar unit contractions remained largely intact, enabling quantification of  $[Ca^{2+}]_i$  responses in basal cells and analysis of the physical distortions to the alveolar units that these cells embrace. These analyses confirmed that increases in  $[Ca^{2+}]_i$  in individual basal cells were temporally correlated with physical distortions to the mechanically compliant luminal cell layer (Fig. 1E and see *SI Appendix, Fig. S5A*). For both the first InsP3 response and the subsequent oscillatory phase, increases in  $[Ca^{2+}]_i$  preceded alveolar unit contractions (Fig. 1F and G and see *SI Appendix, Fig. S5B*). No statistical difference in the firing interval for  $[Ca^{2+}]_i$  was observed between the first and second events and all subsequent events (Fig. 1H). No  $[Ca^{2+}]_i$  oscillations or contractions were observed in live tissue in the absence of OT stimulation (*SI Appendix, Fig. S5C*). These results reveal that each mammary alveolar unit, acting downstream of a basal cell OT/OXTR/InsP3/ $Ca^{2+}$  signaling axis, serves as a biological positive-displacement pump, repeatedly forcing milk out of its central lumen for passage through the ductal network.

**Basal Cell Contractions Are  $Ca^{2+}$  Signal Dependent.** To directly assess  $Ca^{2+}$ -contraction coupling in mammary basal cells, we engineered triple transgenic mice that express GCaMP6f and the red fluorescent protein TdTomato (34) in basal cells (*GCaMP6f-TdTom;K5CreERT2* mice) (Fig. 2A). Using this model, we observed large increases in  $[Ca^{2+}]_i$  in single TdTomato-positive basal cells in response to OT, which immediately preceded their contraction (Fig. 2A–C, see *SI Appendix, Fig. S6*, and *Movie S3*). These data reveal with greater optical clarity how basal cells contract to deform the inner luminal cell layer for milk ejection and show unequivocally, using a second model to measure basal cell contraction, a temporal relationship between the  $Ca^{2+}$  signal and the contractile response (*SI Appendix, Fig. S6B*).

To determine whether  $Ca^{2+}$  forms an essential component of the signal transduction pathway linking OXTR engagement to basal cell contraction, we examined  $[Ca^{2+}]_i$  and contraction events under extracellular  $Ca^{2+}$ -free conditions. Tissue was isolated from pregnant *GCaMP6f-TdTom;K5CreERT2* mice and incubated in a  $Ca^{2+}$ -free physiological salt solution supplemented with the  $Ca^{2+}$  chelator BAPTA. By performing experiments using mammary tissue harvested prior to secretory activation (gestation day 15.5 to 16.5), when  $Ca^{2+}$ -contraction coupling is observed (*Movie S4*), we were able to avoid the exceedingly high (>90 mM) extracellular  $Ca^{2+}$  concentrations present in secreted milk (19). Under these experimental conditions, addition of OT resulted in intracellular  $Ca^{2+}$  store release associated with cell contraction (Fig. 2D and E and *Movie S5*). Ensuing spike trains, however, were absent and subsequent contractions were abolished. Readdition of extracellular  $Ca^{2+}$  led to the resumption of  $Ca^{2+}$  firing and basal cell contractions (Fig. 2D–F). These data demonstrate that both  $Ca^{2+}$  release from InsP3-sensitive intracellular  $Ca^{2+}$  stores (22) and  $Ca^{2+}$  influx across the plasma membrane are sufficient for basal cell contraction but that influx across the membrane is necessary to sustain cell and tissue contractions.

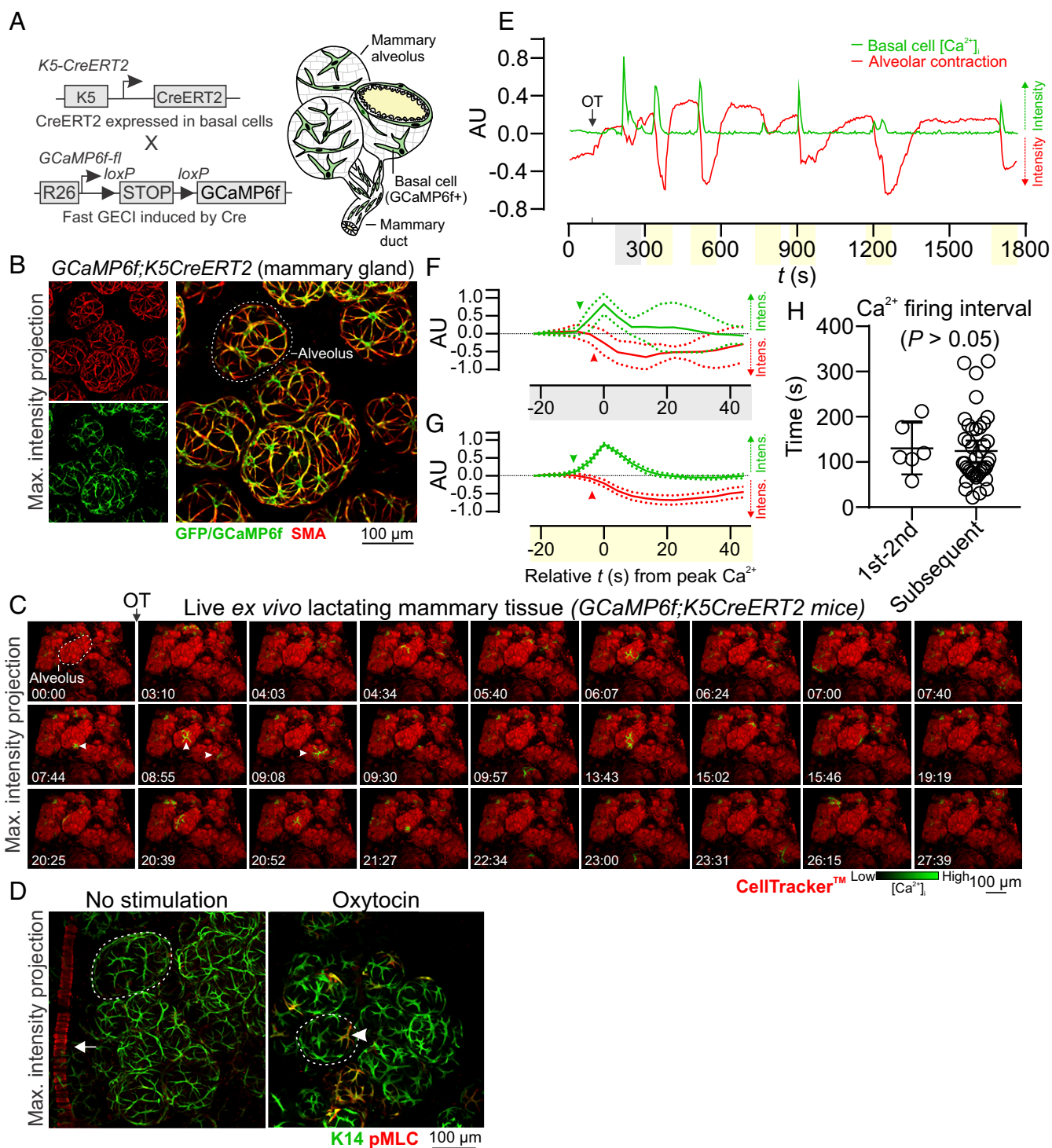


**Fig. 1.** Basal cell Ca<sup>2+</sup> oscillations precede alveolar contractions. (A) Schematic representation of *GCaMP6f;K5CreERT2* model. (B) Maximum intensity z-projection of cleared lactating mammary tissue immunostained with smooth muscle actin (SMA) to reveal basal cells and anti-GFP antibody to detect GCaMP6f. (C) Three-dimensional time-lapse imaging of live mammary tissue from *GCaMP6f;K5CreERT2* lactating mice stimulated with OT (85 nM) at 01:33 (min:s). Images show maximum intensity z-projection. Arrowheads point to Ca<sup>2+</sup> events in single cells. See [Movie S1](#). (D) Maximum intensity z-projections of cleared mammary tissue immunostained with K14 to reveal basal cells and pMLC to show sites of contractile activity. Arrow shows pMLC<sup>+</sup> blood vessel in control tissue, arrowhead shows pMLC<sup>+</sup> basal cell in tissue stimulated with OT (85 nM) prior to fixation; dotted lines surround alveolar units. (E) Quantification of [Ca<sup>2+</sup>]<sub>i</sub> responses (green) and alveolar unit contraction (red) in lactating mammary tissue from *GCaMP6f;K5CreERT2* mice. [Ca<sup>2+</sup>]<sub>i</sub> measurements are  $\Delta F/F_0$ . Alveolar unit contractions shown by negative deflections (CellTracker fluorescence). (F and G) Average ( $\pm$ SEM) peak [Ca<sup>2+</sup>]<sub>i</sub> and contractile responses. Highlighting (x axis) corresponds with events linked in E; arrowheads show initiation of the response. (H) Interval between the first and second, and all subsequent [Ca<sup>2+</sup>]<sub>i</sub> events ( $P > 0.05$ , Student's *t* test). AU, arbitrary unit;  $n = 3$  mice.

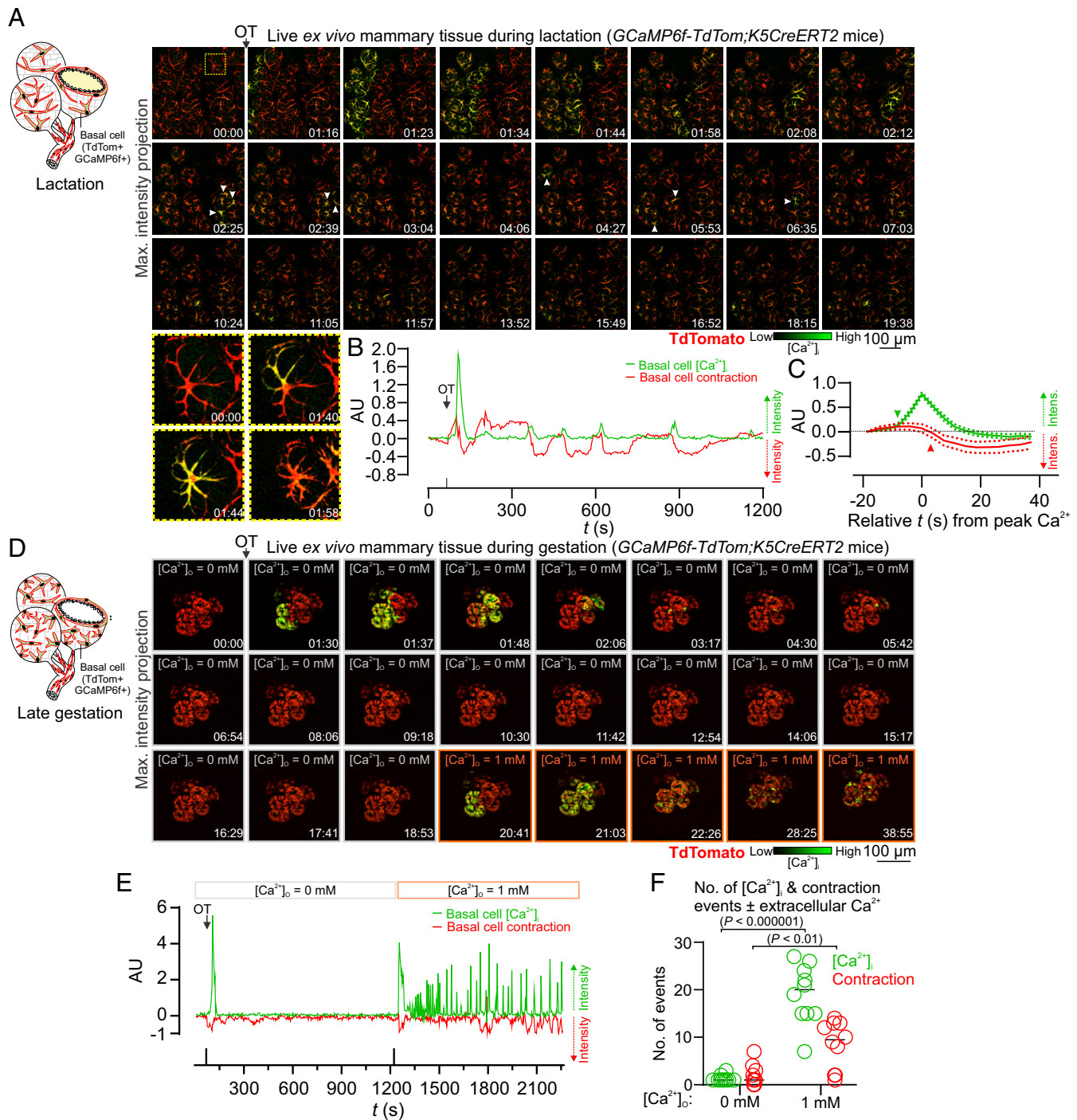


**Fig. 2.** Ca<sup>2+</sup>-contraction coupling. (A) Three-dimensional time-lapse imaging of live mammary tissue from *GCaMP6f-TdTom;K5CreERT2* mice stimulated with OT (85 nM) at 01:09 (min:s). Images show maximum intensity z-projection. Box (frame 1) expanded in panel *Below*; arrowheads point to Ca<sup>2+</sup> events in single cells. See [Movie S3](#). (B) Quantification of [Ca<sup>2+</sup>]<sub>i</sub> responses (green) and alveolar unit contraction (red) in lactating mammary tissue from *GCaMP6f-TdTom;K5CreERT2* mice. [Ca<sup>2+</sup>]<sub>i</sub> measurements are ΔF/F<sub>0</sub>. Basal cell contractions shown by negative deflections (TdTomato fluorescence). (C) Average (±SEM) peak [Ca<sup>2+</sup>]<sub>i</sub> response and contractile response in mammary tissue isolated from lactating *GCaMP6f-TdTom;K5CreERT2* mice. Values averaged from both the first response and the oscillatory phase. (D) Three-dimensional time-lapse imaging of live mammary tissue from *GCaMP6f-TdTom;K5CreERT2* mice (15.5 to 16.5 days postcoitus (d.p.c.) stimulated with OT (85 nM) at 01:08 (min:s) under extracellular Ca<sup>2+</sup> free conditions. Images show maximum intensity z-projection. Ca<sup>2+</sup> (1 mM free Ca<sup>2+</sup>) was added back at 20:23 (min:s). See [Movie S5](#). (E) Quantification of [Ca<sup>2+</sup>]<sub>i</sub> responses and alveolar unit contraction in mammary tissue from pregnant *GCaMP6f-TdTom;K5CreERT2* mice stimulated with OT under extracellular Ca<sup>2+</sup>-free conditions and with Ca<sup>2+</sup> addback. [Ca<sup>2+</sup>]<sub>i</sub> measurements are ΔF/F<sub>0</sub>. Basal cell contractions shown by negative deflections (TdTomato fluorescence). (F) Number of [Ca<sup>2+</sup>]<sub>i</sub> and contraction events ± extracellular Ca<sup>2+</sup> ([Ca<sup>2+</sup>]<sub>o</sub>). Graph shows individual measurements and median. *P* value in parentheses is from multiple *t* tests. *n* = 3 mice.

**Both Ducts and Alveoli Contract to Expel Milk in the Mature Gland.** The lactating mouse mammary gland consists of milk producing alveoli that are connected to the nipple via a branching ductal

network (Fig. 1A). Heterogeneity in the expression of contractile markers in basal cells of ducts and alveoli has led to speculation that these two related (but spatially and morphologically distinct)

cell populations are functionally divergent (35). We compared expression of myosin light chain kinase (MLCK), calponin (CNN1), and caldesmon (CALD1)—key components of the vascular smooth muscle contraction pathway that are up-regulated in the mammary gland during lactation (*SI Appendix, Fig. S7*)—in ducts versus alveoli of lactating mice (Fig. 3*A*) and humans (Fig. 3*B*). Our analyses reveal that these proteins are expressed at comparable levels in basal cells of both structures (Fig. 3*A* and *B* and see *SI Appendix, Fig. S8*).

Next, we used our model to examine possible  $\text{Ca}^{2+}$ -contraction coupling in ductal cells of pregnant *GCaMP6f-TdTom;K5CreERT2* mice. At this developmental stage, contractile proteins are already up-regulated (*SI Appendix, Fig. S7C*),  $\text{Ca}^{2+}$ -contraction coupling is observed in alveolar structures (*Movies S4* and *S5*), and the visualization of ducts is not completely obscured by light scattering and/or absorptive properties of interposing structures. Although oriented deep within the tissue, ductal basal cells responded to OT with a transient increase in  $[\text{Ca}^{2+}]_i$  (Fig. 3*C*) and  $\text{Ca}^{2+}$ -contraction coupling was clearly observed in live recordings (*Movie S6*). Although more challenging to visualize, large ducts that were positioned deep within the mammary tissue of lactating animals were captured (Fig. 3*D* and *Movie S7*), confirming these findings in the fully mature state. In mammary ducts, basal cells adopt a spindle-like morphology and are collectively oriented along the length of the duct (Fig. 1*A*). Our data reveal that contraction of ductal basal cells generates longitudinal motion, facilitating the continued flow of milk. We also demonstrate that differences in the type of motion generated by ductal and alveolar contractions arise from organizational heterogeneity, rather than divergent functional differentiation or signal transduction.

**Mammary Epithelial Cells In Situ Exhibit Both Stochastic and Coordinated Behaviors.** Our model enables us to visualize molecular events in single cells, to observe how these events control an individual cell's behavior, and to understand how individual behaviors produce tissue-level outcomes. In mammary tissue, basal epithelial cells primarily exhibit stochastic activity (Figs. 1 and 2 and see *SI Appendix, Figs. S4* and *S5*). Individual oscillatory behavior, however, was observed to be temporarily entrained across large lobuloalveolar structures (Fig. 3*C* asterisks and see *SI Appendix, Figs. S3* and *S4* asterisks and *Movies S2, S4, and S6*), suggesting that this organ can generate both synchronized and unsynchronized motion for optimal milk ejection. To determine the degree of lobuloalveolar cooperativity in firing, we employed two agnostic approaches to analyze the functional connectivity in  $\text{Ca}^{2+}$  signaling events. First, we analyzed correlations in the firing pattern of individual basal cells in the postdiffusion phase and graphed the Euclidean distances between highly correlated ( $>0.5$ ) cells. Highly correlated responses exhibited a short Euclidean distance (Fig. 3*E*). We also analyzed network topologies by connecting highly correlated cells within a single field of view. This method confirmed high clustering associated with short internodal distances in some lobular structures (small worldness) (*SI Appendix, Fig. S9*) (36, 37). These analyses suggest some cooperativity in firing and, by extension, contraction.

**Distinct Signaling Pathways Underpin the Passage of Milk, Tears, and Sperm.** To assess potential conservation in the signaling pathways that operate in basal cells of other OT-sensitive, fluid-transporting epithelia, we assessed OT-mediated responses in the lacrimal glands and epididymides of *GCaMP6f-TdTom;K5CreERT2* mice. In the lacrimal gland, basal cells have a similar morphology, arrangement, and function to mammary basal cells (38). They have previously been shown to undergo OT-dependent contractions (39), and diminished OT/OXTR signaling in these cells has been linked to dry eye disease (39). Like the mammary gland, dual expression of basal and smooth muscle markers was confirmed in lacrimal acini (Fig. 4*A*); however, no OT-mediated  $[\text{Ca}^{2+}]_i$  or

contractile responses were detected in these cells in this study (Fig. 4*B* and *C* and *Movie S8*).

In males, a large burst of OT is released into the bloodstream at ejaculation (18, 40). This produces contractions of the male reproductive tract and, by assisting with the passage of fluid along this tract, these contractions are thought to reduce postejaculatory refractoriness and improve reproductive readiness (40, 41). Epididymal basal cells express basal cell markers; however, unlike the lacrimal and mammary glands, they do not coexpress smooth muscle markers (Fig. 4*D*). Instead, movement of fluid through this organ appears to rely on a layer of smooth muscle surrounding the inner tubular epithelium (Fig. 4*D*). To assess the transport of sperm through this organ, its OT responsiveness and its relationship to basal cell  $[\text{Ca}^{2+}]_i$  elevations, we stimulated acute epididymal tissue pieces with a large bolus dose of OT. OT stimulation triggered marked peristaltic-like movements of the epididymal tubes (Fig. 4*E*) and a suprabasal pattern of phosphorylation of MLC (*SI Appendix, Fig. S10A*). Low-frequency  $\text{Ca}^{2+}$  firing in basal cells was observed before and after OT stimulation (Fig. 4*F* arrows and see *SI Appendix, Fig. S10B* and *Movie S9*). Basal cell  $\text{Ca}^{2+}$ -contraction signaling can therefore be selectively uncoupled in different fluid moving epithelia.

#### Pharmacological Inhibitors of Regulatory Proteins of Myosin Light Chain Phosphorylation Are Unable to Block Mammary Contractions.

Mammary basal cells typically express smooth muscle actin (*SI Appendix, Fig. S1A*) and strongly up-regulate elements of the vascular smooth muscle contraction pathway during gestation and early lactation (*SI Appendix, Fig. S7*) (7). Our group and others have therefore hypothesized that basal cell contraction is principally controlled by  $\text{Ca}^{2+}$ /calmodulin-dependent phosphorylation of the myosin light chain (MLC) by MLCK and subsequent dephosphorylation by myosin light chain phosphatase (MLCP) (19, 20, 42). This hypothesis is supported in the current study by a pattern of pMLC immunostaining in OT-treated tissue that is consistent with the organization of its  $\text{Ca}^{2+}$  firing activity (Fig. 1*C* and *D* and see *SI Appendix, Fig. S3*). To explore this further, we treated uterine, bladder, epididymal, and mammary tissue pieces with pharmacological inhibitors of both MLCK and the MLCP inhibitor rho-associated protein kinase (ROCK) (*SI Appendix, Fig. S11A*). Inhibition of MLCK and ROCK did not significantly reduce the intensity of tissue contraction in any organ examined (Fig. 5 and *Movie S10*) ( $P > 0.05$ , one-way ANOVA,  $n = 4$ ). This is in contrast to a previous study, which scored contraction based on basal cell morphology in mammary tissue treated prior to fixation with this ROCKi (43). When tissue was incubated with a mixture of pharmacological inhibitors against MLCK, ROCK, protein kinase C (PKC) (44), and  $\text{Ca}^{2+}$ /calmodulin-dependent protein kinase II (CaMKII) (45), however, contraction was robustly inhibited in uterine, epididymal, and bladder preparations ( $53 \pm 13\%$ ,  $69 \pm 12.5\%$ , and  $60 \pm 15\%$  reduction, respectively,  $P < 0.05$ , one-way ANOVA,  $n = 4$ ), but persisted in the mammary gland (Fig. 5*A* and *B* and *Movie S10*), suggesting that other pathways are responsible for mammary basal cell contractions or that they may compensate when these pathways are transiently disrupted.

It is also conceivable, however, that some pharmacological inhibitors are unable to effectively and consistently bind to their intracellular targets when applied to intact, lipid-rich mammary tissue. We therefore interrogated  $\text{Ca}^{2+}$ -contraction coupling in dissociated primary mammary basal cells in a 2D assay. Cells from pregnant *GCaMP6f-TdTom;K5CreERT2* mice were isolated, plated in coculture on a nanopatterned surface (*SI Appendix, Fig. S11B*), and imaged within 12 h of dissection. These conditions were optimal for 1) maintaining cell health and stage-specific differentiation, and 2) achieving anisotropy in the arrangement of contractile elements for the experimental measurement of force generation along a single axis (46). Under

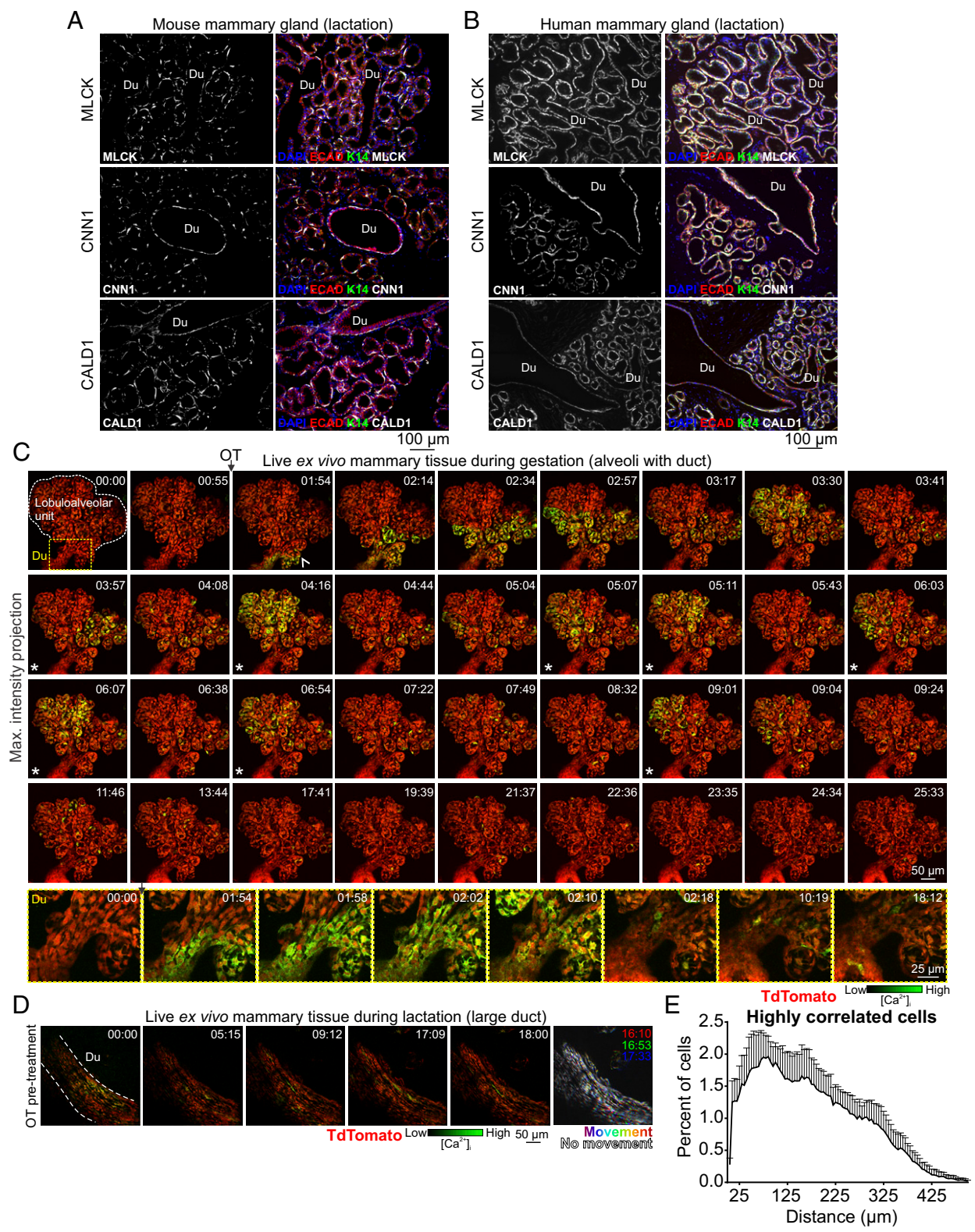


**Fig. 3.** Functional differentiation and  $Ca^{2+}$ -contraction coupling in ducts and alveoli. (*A* and *B*) Immunostaining of paraffin-embedded mouse and human lactating tissue. MLCK, CNN1, and CALD1 are expressed in both ducts (Du) and alveoli. E-cadherin shows the luminal cell lineage; K14 shows the basal cell lineage. Nuclei are stained with DAPI;  $n = 3$  samples, mouse and human. (*C*) Three-dimensional time-lapse imaging of live mammary tissue from a pregnant (15.5 to 16.5 d.p.c.) *GCaMP6f-TdTom;K5CreERT2* mouse stimulated with OT (85 nM) at 01:15 (min:s). Images show maximum intensity z-projection of live tissue; box (frame 1) shows subtending duct (Du, magnified at *Bottom*), extending deeper into the tissue. Arrowhead at 01:54 shows direction of OT diffusion; asterisks show coordinated firing;  $n = 3$ . See *Movie S6*. (*D*) Three-dimensional time-lapse imaging of a large duct from a lactating *GCaMP6f-TdTom;K5CreERT2* mouse stimulated with OT (85 nM) immediately prior to imaging. Images show maximum intensity z-projection of live tissue;  $n = 3$ . See *Movie S7*. (*E*) Percent of cells with a high correlation coefficient ( $>0.5$ ) in  $Ca^{2+}$  firing and the Euclidean distance of correlated events. Graph shows average  $\pm$  SEM ( $n = 4$  mice, gestation).

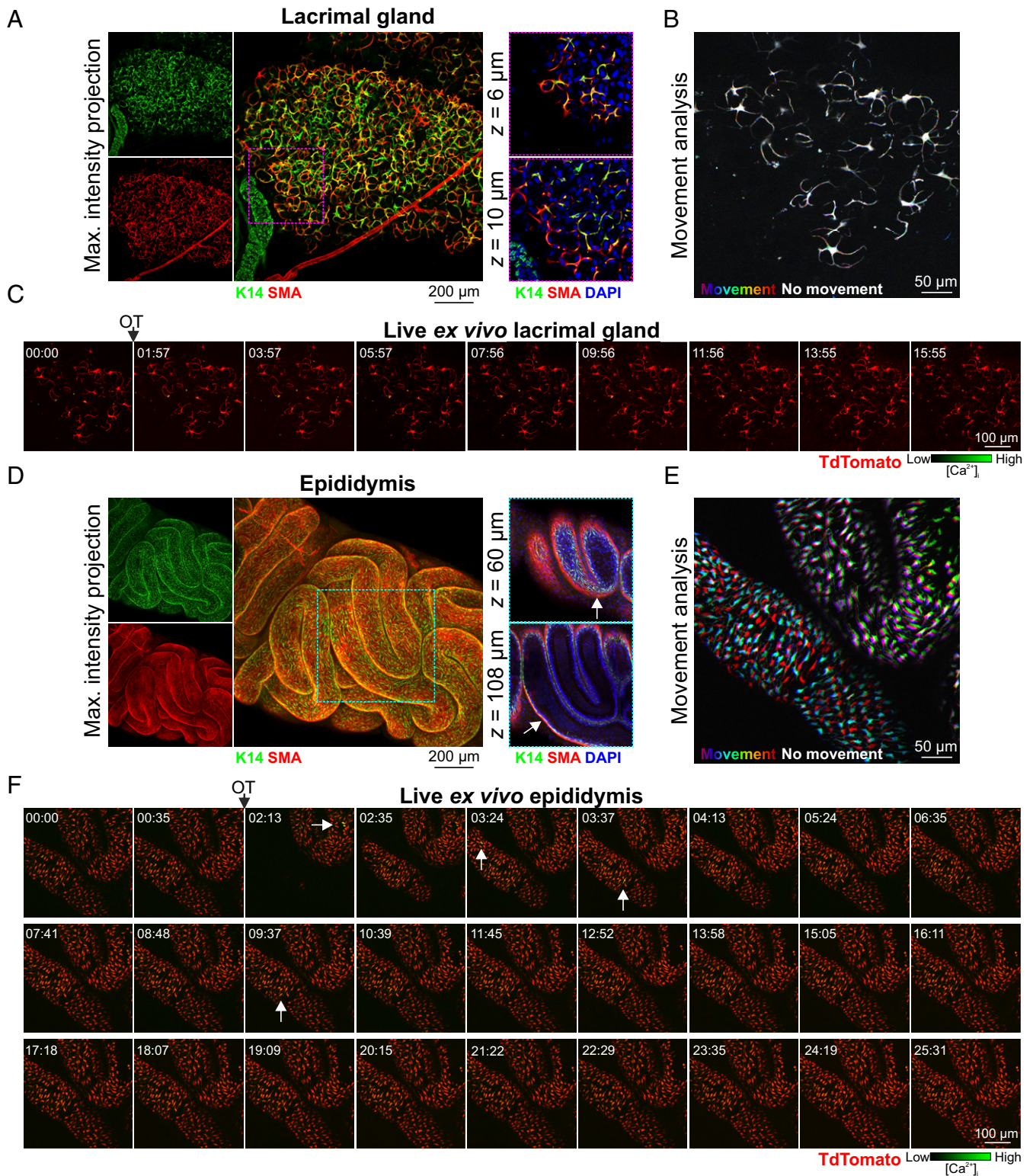


**Fig. 4.** OT responses in basal epithelial cells of other fluid-moving organs. (A) Maximum intensity z-projection and optical slices of lacrimal tissue. Lacrimal acinar basal cells express K14 and SMA. (B) Analysis of tissue movement created by the overlay of three images (approximately 43 s apart). Each image has been assigned a primary color. Regions that do not move during the 90-s window have R-G-B (red, green, and blue) pixels superimposed and are white. Regions where significant movement has occurred appear R, G, B or a combination of two colors. See [Movie S8](#). (C) Three-dimensional time-lapse imaging of lacrimal tissue from *GCaMP6f-TdTom;K5CreERT2* mice. Tissue was stimulated with OT (85 nM, 00:45). Image series show maximum intensity z-projection. (D) Maximum intensity z-projection and optical slices of cleared mouse caput epididymis. Basal K14 positive cells are surrounded by SMA positive cells (arrow). (E) Tissue movement analysis of three images (approximately 45 s apart) as per B. (F) Three-dimensional time-lapse imaging of epididymal tissue from *GCaMP6f-TdTom;K5CreERT2* mice. Tissue was stimulated with OT (850 nM, 01:38); arrows show single-cell calcium responses. See [Movie S9](#). *n* = 3 mice.

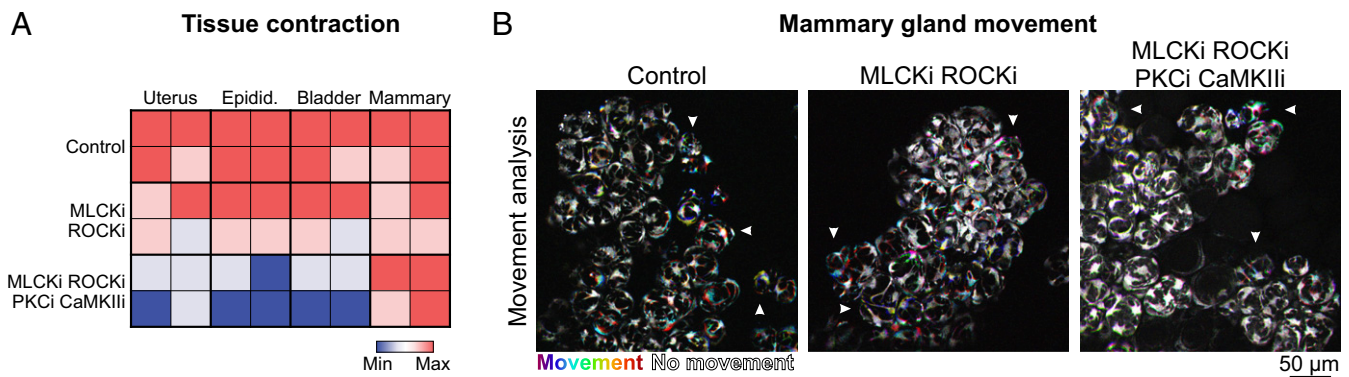


**Fig. 5.** Pharmacological inhibition of the contractile pathway. (A) Matrix of contractile activity in tissue pieces isolated from uterus, epididymis, bladder, and mammary gland and treated with either buffer (control), a combination of inhibitors of MLCK (ML-9) and ROCK (Y27632), or a combination of inhibitors of MLCK (ML-9), ROCK (Y27632), PKC (calphostin-C), and CaMKII (KN93). Contractions were induced with oxytocin (85 nM, uterus and mammary gland; 850 nM epididymis) or carbachol (10  $\mu$ M, bladder). See [Movie S10](#). (B) Analysis of tissue movement in mammary tissue pieces created by the overlay of three images (30 s apart). Each image has been assigned a primary color. Regions that do not move during the 60-s window have R-G-B pixels superimposed and are white. Regions where significant movement has occurred appear R, G, B, or a combination of two colors.  $n = 4$  mice.

these conditions, OT stimulation produced  $[Ca^{2+}]_i$  responses, which were coupled to contraction at the first (InsP3) phase ([SI Appendix, Fig. S11C](#) and [Movie S11](#)). Later phase  $Ca^{2+}$ -contraction coupling, however, was not able to be assessed in this model, due to the intensity of the first contraction (even at picomolar concentrations of OT) and the relatively low strength of the newly formed surface adhesions (22). Nevertheless, as  $Ca^{2+}$ -contraction coupling is observed at this phase, we proceeded to use this system to examine this initial event in primary cells.

Intracellular  $Ca^{2+}$  chelation with BAPTA completely blocked  $[Ca^{2+}]_i$  responses to OT ([SI Appendix, Fig. S11D](#) and [Movie S12](#)). Cell contractions were also attenuated, demonstrating, unequivocally, their  $Ca^{2+}$  dependence. To gauge the distance between the  $Ca^{2+}$  source (in this case InsP3 receptors) and sensor, we compared OT-mediated basal cell contractions in cells loaded with two different  $[Ca^{2+}]_i$  chelators (BAPTA-AM and EGTA-AM), with different  $Ca^{2+}$  binding rates but comparable binding affinities (47, 48). Both intracellular BAPTA and EGTA were able to capture  $Ca^{2+}$  between the channel and the sensor ([SI Appendix, Fig. S11D](#)), suggestive of “loose”  $Ca^{2+}$ -contraction coupling in these cells that is not strictly dependent on nanodomain signaling (where EGTA is ineffective) (48). Similar to whole tissue preparations, however, treatment of cells with MLCK and ROCK inhibitors failed to block OT-mediated basal cell contraction ([SI Appendix, Fig. S11D](#)). These data are not dissimilar to previous studies, where in vitro contraction was inhibited by only 30% in basal cells isolated from mice deficient for the gene encoding smooth muscle actin (42), and support a level of functional redundancy in the mammary contraction pathway.

#### Coupled Oscillator-Based Synchronization in the Mammary Gland.

$Ca^{2+}$ -activation mechanisms in smooth muscle cells are incredibly diverse and are uniquely adapted to match the developmental stage-specific function of the biological structure on which they exert their force. Additional complexity arises when the mechanisms responsible for generating and propagating  $[Ca^{2+}]_i$  signals in “smooth muscle-like” epithelial lineages are considered (49). Here, we demonstrate in mammary basal cells that OXTR engagement produces initial release of  $Ca^{2+}$  from intracellular stores, sufficient to generate cell and tissue contraction. Initial  $[Ca^{2+}]_i$  responses have been shown to be sensitive to PLC inhibition in in vitro assays (22) and similar  $[Ca^{2+}]_i$  responses are observed with InsP3 infusion (22), consistent with coupling via  $G_q$  proteins to PLC $\beta$  (18). In some smooth muscle cells,  $[Ca^{2+}]_i$  signals are propagated along the length of the cell

via the regenerative release of stored  $Ca^{2+}$  by ryanodine receptors (RYRs) (50, 51). As cytosolic  $Ca^{2+}$  waves were also observed in mammary basal cells (Fig. 2A), we investigated novel roles for RYRs in this tissue. *Ryr1* (but not -2 or -3) was expressed in lysates that were prepared from homogenized mammary tissue during lactation ([SI Appendix, Fig. S12A](#)) and enriched in functionally mature basal cells ([SI Appendix, Fig. S12B](#)). To determine the role of RYR1 channels in these cells, we treated mammary tissue from *GCaMP6f-TdTom;K5CreERT2* mice with the ryanodine receptor inhibitor dantrolene (52). Dantrolene did not inhibit the initial release of  $Ca^{2+}$  from intracellular stores (Fig. 6A temporal sequence 1 and [Movie S13](#)). However, to our surprise,  $[Ca^{2+}]_i$  oscillations became entrained in some regions and tissue exhibited rhythmic and sustained pulses of activity that resembled smooth muscle phase waves, with a periodicity (time between waves) of  $104.2 \pm 16.38$  s and a velocity (speed of wave through the tissue) of  $10.62 \pm 2.64$   $\mu$ m $\cdot$ s $^{-1}$  (Fig. 6A temporal sequence 2, Fig. 6B and [Movie S13](#)). A similar effect was observed with inhibiting concentrations of the plant alkaloid ryanodine (53) ([Movie S14](#)). These data, together with our observation that  $[Ca^{2+}]_i$  oscillations could be temporarily entrained under physiological conditions (Fig. 3C and see [SI Appendix, Fig. S4](#) and [Movies S2](#) and [S6](#)), support a model whereby mammary basal cells can alternate between unsynchronized movements and coupled oscillator-based lobuloalveolar synchronization, modulated in part by the mechanism of ER  $Ca^{2+}$  release.

A key factor of coupled oscillator-based synchronization is intercellular communication via gap junctions (50, 54). Mammary basal cells express Cx43 (55, 56) and mice with severely compromised Cx43 function have impaired milk ejection (57). However, it is often difficult to appreciate how stellate basal cells are physically coupled to their neighbors when visualized using thin tissue sections ([SI Appendix, Fig. S13](#)). Similarly, due to their size and exclusion from near plasma membrane domains, the true extent of basal cell connectivity has not yet been captured using three-dimensional imaging of conventional basal cell markers ([SI Appendix, Fig. S14](#)). To overcome this, we developed mice that express a membrane localized fluorescent protein in basal cells and assessed Cx43 localization in optically cleared tissue. Using this approach, basal cell boundaries were readily identified, enabling us to visualize how thin processes of adjacent cells are physically connected (Fig. 6C, *Top*). Cx43 was enriched at sites of homotypic cell contact (Fig. 6C, *Bottom* arrows). These data confirm that the cytoplasm of adjacent basal cells



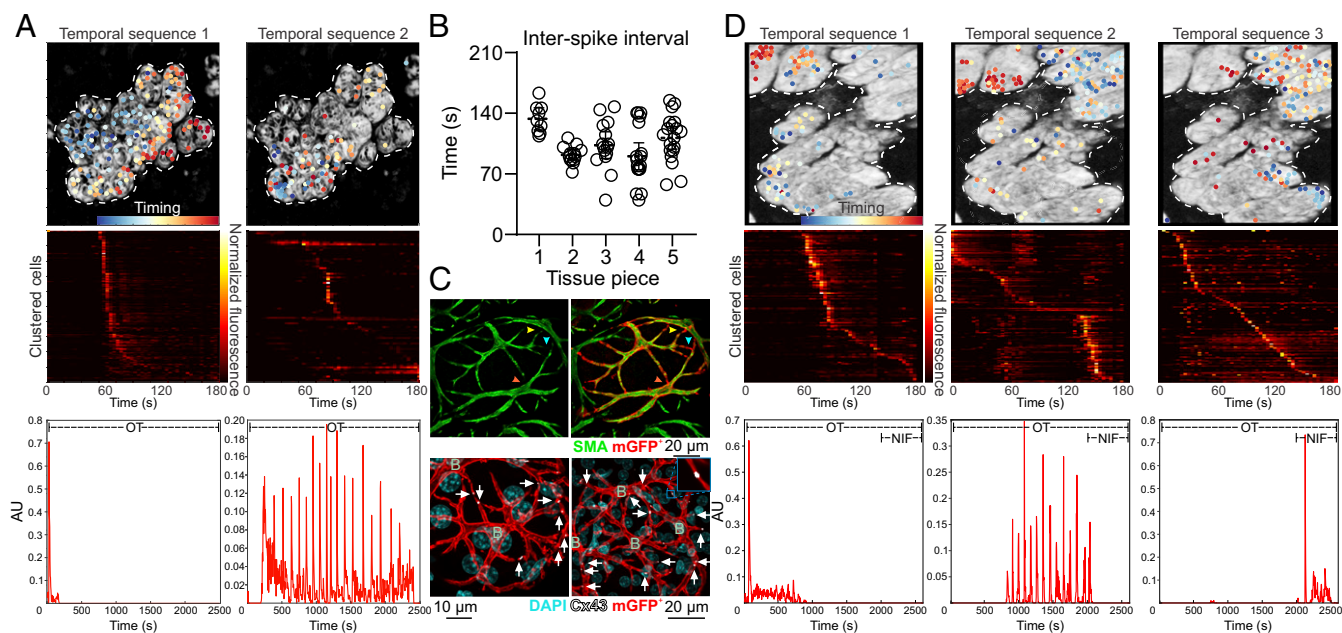


**Fig. 6.** Dantrolene-induced tissue synchronization. (A) Sequential non-negative matrix factorization (seqNMF) was used for unsupervised discovery of repeated temporal sequences of activation and to cluster cells accordingly. Temporal sequence 1 corresponds to the initial InsP3 response; temporal sequence 2 corresponds to the dantrolene-dependent synchronized oscillations. Dots (*Top*) are cells color coded (see timing colorbar) according to the order of their activation in the sequence (*Middle*, each row is one cell) and overlaid on a maximum intensity z-projection of the green channel. The times at which each temporal sequence of  $[Ca^{2+}]_i$  activity is repeated for each cluster is represented by a spike at the *Bottom*;  $n = 3$  mice. (B) Interval between each synchronized oscillation in ex vivo dantrolene-treated mammary tissue (mean  $\pm$  95% CI);  $n = 5$  tissue pieces from at least 3 mice. (C) Optically cleared mammary tissue from lactating mice showing SMA immunostaining (green, *Top*) and cells expressing a membrane-targeted fluorescent protein (red, *Top*). Colored arrowheads point to sites of cell-cell contact that are revealed by the membrane fluorescent protein (Lck-GCaMP6f/mGFP, detected using an anti-GFP antibody). Immunostaining for Cx43 (white, *Bottom*) in cells expressing the membrane-targeted fluorescent protein (red, *Bottom*). White arrows show Cx43 staining at sites where basal cells are connected; B, basal cell;  $n = 3$  mice. (D) seqNMF as in A, where temporal sequence 1 corresponds to the initial InsP3 response; temporal sequence 2 corresponds to dantrolene-dependent synchronized oscillations; and temporal sequence 3 corresponds to addition of nifedipine. After addition of nifedipine, the synchronized activity disappears and switches to a stochastic activity distributed through the tissue, as can be seen by the lack of repeated spikes in the bottom pane. See [Movie S15](#).  $n = 3$  mice.

are linked, enabling individual cells to coordinate the activity of the larger system.

In other tissue types that exhibit rhythmic contractions, e.g., vascular, lymphatic, and airway smooth muscle, periodic release of  $Ca^{2+}$  from the ER produces membrane depolarization and activation of L-type  $Ca^{2+}$  channels (50). Current flow through gap junctions enables depolarization to spread rapidly into neighboring cells, synchronizing large numbers of cells potentially over millimeter distances (50, 54). To determine whether L-type calcium channels are involved in synchronization events in the mammary gland, we treated rhythmically contracting tissue with the L-type  $Ca^{2+}$  channel blocker nifedipine. Nifedipine rapidly and consistently resulted in the reversion to stochastic activity (Fig. 6D [absence of repeated sequences of activation for temporal sequence 3] and [Movie S15](#)). Collectively, these data reveal that mammary basal cells are physically and electrically coupled, enabling  $Ca^{2+}$  to control both the behavior of individual cells as well as the system as a whole.

## Discussion

Real-time, in situ activity monitoring provides important insights into how individual cells behave in multidimensional and multicellular environments (12–15). This approach was used to describe and quantify the mechanism by which milk is transported through the hollow mammary epithelium, making it available on demand and with minimal delay to the nursing neonate (2, 18). Our data support a number of conclusions that could not have been obtained using conventional methods.

We revealed that transient  $[Ca^{2+}]_i$  elevations precede and are required for basal cell contractions in the functionally mature gland. We extended this finding to demonstrate how  $Ca^{2+}$ -contraction coupling in a single basal cell can physically warp the layer of alveolar luminal cells that it encircles. Structure, function, and expression were examined in the adjoining ductal epithelium, previously relegated to a role akin to a biological drinking straw. Instead, our analyses revealed active participation of the ductal epithelium in the process of milk ejection. Differences in the type of motion generated by basal cell contractions in ducts and alveoli were ascribed to heterogeneity in cellular organization, rather than expression or function of contractile elements.

We explored components of the contractile network downstream of  $Ca^{2+}$  activation in mammary basal cells. A pattern of pMLC positivity was observed in mammary cell ensembles, which mirrored the  $Ca^{2+}$  activity of the tissue. Pharmacological inhibition of the  $Ca^{2+}$ -dependent MLCK and the  $Ca^{2+}$ -sensitizer ROCK, however, failed to block mammary contractions in our study. While MLCK is widely considered to be the primary  $Ca^{2+}$ -dependent regulator of MLC phosphorylation in smooth muscle, this model is based on reductionist principles, does not fit all smooth muscle cell types, and fails to acknowledge the growing complexity in regulatory kinases known or hypothesized to govern smooth muscle contraction in vivo (58–60). Indeed, embryonic blood vessels from MLCK knockout mice remain responsive to cytosolic  $Ca^{2+}$  elevations (61). Our data reveal that, similar to aortic smooth muscle cells, smooth muscle-like epithelial cells in the mammary gland also display considerable complexity and diversity in their biomechanical behavior. Complexity in the

pathways downstream of  $\text{Ca}^{2+}$  activation may extend beyond  $\text{Ca}^{2+}$ -contraction coupling to  $\text{Ca}^{2+}$ -transcription coupling (62), an aspect of signaling that has not been considered here but which may be relevant for the interpretation of genetic knockout models (19).

In addition to the diversity in signal transduction downstream of  $\text{Ca}^{2+}$  activation in mammary basal cells, our study and others (19, 22, 63) have demonstrated that a number of  $\text{Ca}^{2+}$  channels—with distinct activation mechanisms and cellular localizations—participate in its encoding. These include channels that regulate  $\text{Ca}^{2+}$  release from intracellular stores, influx from the extracellular environment, and movement between the cytosol of adjacent cells. In this sense,  $[\text{Ca}^{2+}]_i$  acts as a central node in a type of bow-tie motif in basal cells (64), whereby multiplicity in its encoding and decoding enable this evolutionarily essential organ to engage local and global motions to ensure adequate nutrition for the dependent offspring, while on the other hand remaining vulnerable at this crucial point of convergence.

The dynamic nature of the oscillatory  $\text{Ca}^{2+}$  signal enables basal cells to rapidly cycle between contracted and relaxed states. We posit that the spatiotemporal properties of this signal are important inasmuch as its oscillation intensity and interval match the activation threshold and decay rate of the downstream effector to permit efficient switching between cycles of contraction and relaxation. Coupling of the  $\text{Ca}^{2+}$  sensor within nanometer distance to the channel pore, however, appears unlikely based on the following observations: 1) both ER  $\text{Ca}^{2+}$  release and plasmalemmal  $\text{Ca}^{2+}$  influx were sufficient for in situ basal cells to develop and bear tension; and 2) BAPTA-AM and EGTA-AM were equally effective in inhibiting in vitro contractions, despite EGTA's slower binding kinetics. Although not essential for  $\text{Ca}^{2+}$ -contraction coupling, highly spatially regulated  $[\text{Ca}^{2+}]_i$  signals may be an important factor for  $\text{Ca}^{2+}$ -transcription coupling for the long-term maintenance of the contractile phenotype (62) or  $\text{Ca}^{2+}$  wave generation at the tissue level.

Finally, our data, together with published work, suggest that mammary basal cells are able to shift between store- (19) and voltage-dependent modes of operation, a phenomenon that appears to be moderated, at least in part, by the mechanism of ER  $\text{Ca}^{2+}$  release. It is currently unclear how basal cells coordinate the activity of these two, often reciprocally regulated (65, 66), influx pathways under physiological conditions. However, our observation that pharmacological inhibition of RYR1 promoted dihydropyridine-sensitive signal synchronization, corresponds with accounts of RYR activity in bona fide smooth muscle cells (62). Here, RYR-mediated  $\text{Ca}^{2+}$  sparks can activate nearby  $\text{BK}_{\text{Ca}}$  channels, producing spontaneous transient outward currents (STOCs), membrane hyperpolarization, and reduced  $\text{Ca}_v1.2$  activity (50, 62). Optical monitoring of voltage in three dimensions using genetically encoded voltage indicators (GEVIs) (67) and examination of population dynamics in *Cacna1c*-, *Ryr1*-, and

*Kcnma1*-conditional knockout mice remain aims for the future. It is also unclear at this time whether spatial synchronicity can be initiated by any oscillating basal cell (alveolar or ductal) within the mammary epithelium or whether basal cells lock into the frequency of a putative population of epithelial (68) or interstitial (69) mammary “pacemaker” cells. This question may be addressed by future studies using light-sheet fluorescence microscopy and quantitative image analysis to create a spatial footprint of the frequency dynamics of individual oscillators and phase advanced cells.

In summary, by imaging activity in the mammary gland across scales, we were able to visualize and describe in unprecedented detail how the repetitive and collective effort of thousands of mammary basal cells facilitate the transport of a thick biological emulsion through a narrow passage in a manner that is both consistent and persistent. Moreover, the system presented here represents a physiologically relevant model for studying the collective nature of mammalian biological processes.

## Materials and Methods

**Mice.** Animal experimentation was carried out in accordance with the Australian Code for the Care and Use of Animals for Scientific Purposes and the Queensland Animal Care and Protection Act (2001), with local animal ethics committee approval. Strain, genotyping, and reporter induction methods are detailed in *SI Appendix*.

**Human Subjects.** Healthy tissue biopsies from consented lactating women were obtained from the Susan G. Komen Tissue Bank at the IU Simon Cancer Center; see *SI Appendix*.

**Ex Vivo Tissue Imaging.** Mammary glands and uteri were harvested from lactating wild-type, *GCaMP6f;K5CreERT2*, or *GCaMP6f-TdTom;K5CreERT2* mice, diced into 3- to 4-mm<sup>3</sup> pieces and loaded with CellTracker (1.5  $\mu\text{M}$ ) in complete media for at least 20 min at 37 °C and 5%  $\text{CO}_2$  (19). Under these conditions CellTracker preferentially labels luminal cells (*SI Appendix, Fig. S1A*). Images were acquired using an Olympus FV3000 laser scanning microscope; see *SI Appendix* for details and intravital imaging conditions.

**Statistical Analysis.** Statistical analysis was performed in GraphPad Prism (v7.03). Details of statistical tests are outlined in the figure legends.

**Data Availability.** All data are available in the article and *SI Appendix*. Scripts are available on GitHub, [https://github.com/NickCondon/FMD\\_Cell\\_Contraction\\_Script](https://github.com/NickCondon/FMD_Cell_Contraction_Script) (70).

**ACKNOWLEDGMENTS.** This work was supported by the National Health and Medical Research Council (1141008, 1138214), The University of Queensland, the Mater Foundation (Equity Trustees/AE Hingeley Trust), and the National Stem Cell Foundation of Australia. We thank Dr. Jerome Boulanger for the 3D denoising algorithm and Mr. Karsten Bach for assistance with accessing and analyzing RNA-sequencing data. Samples from the Komen Tissue Bank at the IU Simon Cancer Center were used in this study; we thank contributors, donors, and their families.

1. C. G. Victora *et al.*; Lancet Breastfeeding Series Group, Breastfeeding in the 21st century: Epidemiology, mechanisms, and lifelong effect. *Lancet* **387**, 475–490 (2016).
2. H. Macias, L. Hinck, Mammary gland development. *Wiley Interdiscip. Rev. Dev. Biol.* **1**, 533–557 (2012).
3. P. Cowin, J. Wysolmerski, Molecular mechanisms guiding embryonic mammary gland development. *Cold Spring Harb. Perspect. Biol.* **2**, a003251 (2010).
4. B. Lloyd-Lewis, O. B. Harris, C. J. Watson, F. M. Davis, Mammary stem cells: Premise, properties and perspectives. *Trends Cell Biol.* **27**, 556–567 (2017).
5. K. E. Sleeman *et al.*, Dissociation of estrogen receptor expression and in vivo stem cell activity in the mammary gland. *J. Cell Biol.* **176**, 19–26 (2007).
6. A. Van Keymeulen *et al.*, Lineage-restricted mammary stem cells sustain the development, homeostasis, and regeneration of the estrogen receptor positive lineage. *Cell Rep.* **20**, 1525–1532 (2017).
7. K. Bach *et al.*, Differentiation dynamics of mammary epithelial cells revealed by single-cell RNA sequencing. *Nat. Commun.* **8**, 2128 (2017).
8. A. Van Keymeulen *et al.*, Distinct stem cells contribute to mammary gland development and maintenance. *Nature* **479**, 189–193 (2011).
9. B. Lloyd-Lewis, F. M. Davis, O. B. Harris, J. R. Hitchcock, C. J. Watson, Neutral lineage tracing of proliferative embryonic and adult mammary stem/progenitor cells. *Development* **145**, 164079 (2018).
10. F. M. Davis *et al.*, Single-cell lineage tracing in the mammary gland reveals stochastic clonal dispersion of stem/progenitor cell progeny. *Nat. Commun.* **7**, 13053 (2016).
11. N. Gjorevski, C. M. Nelson, Integrated morphodynamic signalling of the mammary gland. *Nat. Rev. Mol. Cell Biol.* **12**, 581–593 (2011).
12. M. Toyota *et al.*, Glutamate triggers long-distance, calcium-based plant defense signaling. *Science* **361**, 1112–1115 (2018).
13. L. A. L. Heap, G. Vanwalleghem, A. W. Thompson, I. A. Favre-Bulle, E. K. Scott, Luminance changes drive directional startle through a thalamic pathway. *Neuron* **99**, 293–301.e4 (2018).
14. T. W. Dunn *et al.*, Neural circuits underlying visually evoked escapes in larval zebrafish. *Neuron* **89**, 613–628 (2016).
15. J. Cichon, W. B. Gan, Branch-specific dendritic  $\text{Ca}^{2+}$  spikes cause persistent synaptic plasticity. *Nature* **520**, 180–185 (2015).
16. T.-W. Chen *et al.*, Ultrasensitive fluorescent proteins for imaging neuronal activity. *Nature* **499**, 295–300 (2013).
17. Q. Chen *et al.*, Imaging neural activity using Thy1-GCaMP transgenic mice. *Neuron* **76**, 297–308 (2012).
18. G. Gimpl, F. Fahrenholz, The oxytocin receptor system: Structure, function, and regulation. *Physiol. Rev.* **81**, 629–683 (2001).

19. F. M. Davis *et al.*, Essential role of Orai1 store-operated calcium channels in lactation. *Proc. Natl. Acad. Sci. U.S.A.* **112**, 5827–5832 (2015).
20. D. M. Moore, A. W. Vogl, K. Baimbridge, J. T. Emerman, Effect of calcium on oxytocin-induced contraction of mammary gland myoepithelium as visualized by NBD-phalloidin. *J. Cell Sci.* **88**, 563–569 (1987).
21. G. M. Oliins, R. D. Bremel, Oxytocin-stimulated myosin phosphorylation in mammary myoepithelial cells: Roles of calcium ions and cyclic nucleotides. *Endocrinology* **114**, 1617–1626 (1984).
22. H. Nakano, K. Furuya, S. Yamagishi, Synergistic effects of ATP on oxytocin-induced intracellular Ca<sup>2+</sup> response in mouse mammary myoepithelial cells. *Pflugers Arch.* **442**, 57–63 (2001).
23. H. J. Lee, H. K. Caldwell, A. H. Macbeth, S. G. Tolu, W. S. Young 3rd, A conditional knockout mouse line of the oxytocin receptor. *Endocrinology* **149**, 3256–3263 (2008).
24. K. Nishimori *et al.*, Oxytocin is required for nursing but is not essential for parturition or reproductive behavior. *Proc. Natl. Acad. Sci. U.S.A.* **93**, 11699–11704 (1996).
25. Y. Takayanagi *et al.*, Pervasive social deficits, but normal parturition, in oxytocin receptor-deficient mice. *Proc. Natl. Acad. Sci. U.S.A.* **102**, 16096–16101 (2005).
26. H. Dana *et al.*, High-performance calcium sensors for imaging activity in neuronal populations and microcompartments. *Nat. Methods* **16**, 649–657 (2019).
27. R. Srinivasan *et al.*, New transgenic mouse lines for selectively targeting astrocytes and studying calcium signals in astrocyte processes in situ and in vivo. *Neuron* **92**, 1181–1195 (2016).
28. B. Lloyd-Lewis *et al.*, Imaging the mammary gland and mammary tumours in 3D: Optical tissue clearing and immunofluorescence methods. *Breast Cancer Res.* **18**, 127 (2016).
29. W. Akemann, H. Mutoh, A. Perron, J. Rossier, T. Knöpfel, Imaging brain electric signals with genetically targeted voltage-sensitive fluorescent proteins. *Nat. Methods* **7**, 643–649 (2010).
30. G. Dupont, L. Combettes, G. S. Bird, J. W. Putney, Calcium oscillations. *Cold Spring Harb. Perspect. Biol.* **3**, a004226 (2011).
31. A. Masedunskas, Y. Chen, R. Stussman, R. Weigert, I. H. Mather, Kinetics of milk lipid droplet transport, growth, and secretion revealed by intravital imaging: Lipid droplet release is intermittently stimulated by oxytocin. *Mol. Biol. Cell* **28**, 935–946 (2017).
32. B. B. Avants *et al.*, A reproducible evaluation of ANTs similarity metric performance in brain image registration. *Neuroimage* **54**, 2033–2044 (2011).
33. B. B. Avants, C. L. Epstein, M. Grossman, J. C. Gee, Symmetric diffeomorphic image registration with cross-correlation: Evaluating automated labeling of elderly and neurodegenerative brain. *Med. Image Anal.* **12**, 26–41 (2008).
34. T. X. Dong *et al.*, T-cell calcium dynamics visualized in a ratiometric tdTomato-GCaMP6f transgenic reporter mouse. *eLife* **6**, e32417 (2017).
35. M. Moumen *et al.*, The mammary myoepithelial cell. *Int. J. Dev. Biol.* **55**, 763–771 (2011).
36. A. Stozer *et al.*, Functional connectivity in islets of Langerhans from mouse pancreas tissue slices. *PLOS Comput. Biol.* **9**, e1002923 (2013).
37. D. J. Watts, S. H. Strogatz, Collective dynamics of “small-world” networks. *Nature* **393**, 440–442 (1998).
38. D. T. Farmer *et al.*, Defining epithelial cell dynamics and lineage relationships in the developing lacrimal gland. *Development* **144**, 2517–2528 (2017).
39. D. Hawley *et al.*, Myoepithelial cell-driven acini contraction in response to oxytocin receptor stimulation is impaired in lacrimal glands of Sjögren’s syndrome animal models. *Sci. Rep.* **8**, 9919 (2018).
40. H. Thackare, H. D. Nicholson, K. Whittington, Oxytocin—its role in male reproduction and new potential therapeutic uses. *Hum. Reprod. Update* **12**, 437–448 (2006).
41. S. Arrighi, Are the basal cells of the mammalian epididymis still an enigma? *Reprod. Fertil. Dev.* **26**, 1061–1071 (2014).
42. C. J. Haaksma, R. J. Schwartz, J. J. Tomasek, Myoepithelial cell contraction and milk ejection are impaired in mammary glands of mice lacking smooth muscle alpha-actin. *Biol. Reprod.* **85**, 13–21 (2011).
43. K. Raymond *et al.*, Control of mammary myoepithelial cell contractile function by  $\alpha 3 \beta 1$  integrin signalling. *EMBO J.* **30**, 1896–1906 (2011).
44. I. Y. Kuo, B. E. Ehrlich, Signaling in muscle contraction. *Cold Spring Harb. Perspect. Biol.* **7**, a006023 (2015).
45. A. Rokolya, H. A. Singer, Inhibition of CaM kinase II activation and force maintenance by KN-93 in arterial smooth muscle. *Am. J. Physiol. Cell Physiol.* **278**, C537–C545 (2000).
46. S. Chaterji *et al.*, Synergistic effects of matrix nanotopography and stiffness on vascular smooth muscle cell function. *Tissue Eng. Part A* **20**, 2115–2126 (2014).
47. N. P. Vyleta, P. Jonas, Loose coupling between Ca<sup>2+</sup> channels and release sensors at a plastic hippocampal synapse. *Science* **343**, 665–670 (2014).
48. E. Eggemann, I. Bucurenciu, S. P. Goswami, P. Jonas, Nanodomain coupling between Ca<sup>2+</sup> channels and sensors of exocytosis at fast mammalian synapses. *Nat. Rev. Neurosci.* **13**, 7–21 (2011).
49. K. C. Richardson, Contractile tissues in the mammary gland, with special reference to myoepithelium in the goat. 1949. *J. Mammary Gland Biol. Neoplasia* **14**, 223–242 (2009).
50. M. J. Berridge, Smooth muscle cell calcium activation mechanisms. *J. Physiol.* **586**, 5047–5061 (2008).
51. M. L. Collier, G. Ji, Y. Wang, M. I. Kotlikoff, Calcium-induced calcium release in smooth muscle: Loose coupling between the action potential and calcium release. *J. Gen. Physiol.* **115**, 653–662 (2000).
52. R. H. Choi, X. Koenig, B. S. Launikonis, Dantrolene requires Mg<sup>2+</sup> to arrest malignant hyperthermia. *Proc. Natl. Acad. Sci. U.S.A.* **114**, 4811–4815 (2017).
53. G. Meissner, Ryanodine activation and inhibition of the Ca<sup>2+</sup> release channel of sarcoplasmic reticulum. *J. Biol. Chem.* **261**, 6300–6306 (1986).
54. M. S. Imtiaz, P. Y. von der Weid, D. F. van Helden, Synchronization of Ca<sup>2+</sup> oscillations: A coupled oscillator-based mechanism in smooth muscle. *FEBS J.* **277**, 278–285 (2010).
55. R. Mroue, J. Inman, J. Mott, I. Budunova, M. J. Bissell, Asymmetric expression of connexins between luminal epithelial- and myoepithelial- cells is essential for contractile function of the mammary gland. *Dev. Biol.* **399**, 15–26 (2015).
56. R. S. Talhouk *et al.*, Developmental expression patterns and regulation of connexins in the mouse mammary gland: Expression of connexin30 in lactogenesis. *Cell Tissue Res.* **319**, 49–59 (2005).
57. M. K. G. Stewart *et al.*, The severity of mammary gland developmental defects is linked to the overall functional status of Cx43 as revealed by genetically modified mice. *Biochem. J.* **449**, 401–413 (2017).
58. P. H. Ratz, Inhibitor  $\kappa$ B kinase: Another node in the cell signaling network regulating smooth muscle contraction. *Circ. Res.* **113**, 484–486 (2013).
59. Z. Ying *et al.*, Inhibitor  $\kappa$ B kinase 2 is a myosin light chain kinase in vascular smooth muscle. *Circ. Res.* **113**, 562–570 (2013).
60. M. V. Artamonov *et al.*, RSK2 contributes to myogenic vasoconstriction of resistance arteries by activating smooth muscle myosin and the Na<sup>+</sup>/H<sup>+</sup> exchanger. *Sci. Signal* **11**, eaar3924 (2018).
61. A. V. Somlyo *et al.*, Myosin light chain kinase knockout. *J. Muscle Res. Cell Motil.* **25**, 241–242 (2004).
62. D. C. Hill-Eubanks, M. E. Werner, T. J. Heppner, M. T. Nelson, Calcium signaling in smooth muscle. *Cold Spring Harb. Perspect. Biol.* **3**, a004549 (2011).
63. H. Nakano, K. Furuya, S. Furuya, S. Yamagishi, Involvement of P2-purinergic receptors in intracellular Ca<sup>2+</sup> responses and the contraction of mammary myoepithelial cells. *Pflugers Arch.* **435**, 1–8 (1997).
64. P. A. Brodskiy, J. J. Zartman, Calcium as a signal integrator in developing epithelial tissues. *Phys. Biol.* **15**, 051001 (2018).
65. Y. Wang *et al.*, The calcium store sensor, STIM1, reciprocally controls Orai and CaV1.2 channels. *Science* **330**, 105–109 (2010).
66. C. Y. Park, A. Shcheglovitov, R. Dolmetsch, The CRAC channel activator STIM1 binds and inhibits L-type voltage-gated calcium channels. *Science* **330**, 101–105 (2010).
67. V. Villette *et al.*, Ultrafast two-photon imaging of a high-gain voltage indicator in awake behaving mice. *Cell* **179**, 1590–1608.e23 (2019).
68. B. F. De Blasio, J. G. Iversen, J. A. Røttingen, Intercellular calcium signalling in cultured renal epithelia: A theoretical study of synchronization mode and pacemaker activity. *Eur. Biophys. J.* **33**, 657–670 (2004).
69. M. Gherghiceanu, L. M. Popescu, Interstitial Cajal-like cells (ICLC) in human resting mammary gland stroma. Transmission electron microscope (TEM) identification. *J. Cell. Mol. Med.* **9**, 893–910 (2005).
70. N. D. Condon, FMD cell contraction script. GitHub. [https://github.com/NickCondon/FMD\\_Cell\\_Contraction\\_Script](https://github.com/NickCondon/FMD_Cell_Contraction_Script). Deposited 4 June 2019.